

# LLM-Flock: Decentralized Multi-Robot Flocking via Large Language Models and Influence-Based Consensus

**Peihan Li**

Drexel University,  
United States  
pl1525@drexel.edu

**Lifeng Zhou\***

Drexel University,  
United States  
lz457@drexel.edu

**Abstract:** Large Language Models (LLMs) have advanced rapidly in recent years, demonstrating strong capabilities in problem comprehension and reasoning. Inspired by these developments, researchers have begun exploring the use of LLMs as decentralized decision-makers for multi-robot formation control. However, prior studies reveal that directly applying LLMs to such tasks often leads to unstable and inconsistent behaviors—robots may collapse to the centroid of their positions or diverge entirely—due to hallucinated reasoning, logical inconsistencies, and limited coordination awareness. To overcome these limitations, we propose a novel framework that integrates LLMs with an influence-based plan consensus protocol. In this framework, each robot independently generates a local plan toward the desired formation using its own LLM. The robots then iteratively refine their plans through a decentralized consensus protocol that accounts for their influence on neighboring robots. This process drives the system toward a coherent and stable flocking formation in a fully decentralized manner. We evaluate our approach through comprehensive simulations involving both state-of-the-art closed-source LLMs (e.g., o3-mini, Claude 3.5) and open-source models (e.g., Llama3.1-405b, Qwen-Max, DeepSeek-R1). The results show notable improvements in stability, convergence, and adaptability over previous LLM-based methods. We further validate our framework on a physical team of Crazyflie drones, demonstrating its practical viability and effectiveness in real-world multi-robot systems. The video<sup>2</sup> and code<sup>3</sup> are available online.

**Keywords:** Multi-Robot Systems, Flocking, Large Language Models, Influence-Based Consensus

## 1 Introduction

Decentralized formation control in multi-robot systems has been a popular topic over the decades [1, 2]. Enabling a team of robots to coordinate and maintain desired formations without centralized control is critical for applications such as environmental monitoring, search-and-rescue missions, and distributed exploration [3, 4, 5, 6, 7]. Classical decentralized control strategies, including rule-based flocking algorithms and graph-based consensus methods, achieve global coordination through local interactions [8, 9]. However, these approaches often rely on simple heuristics or static interaction models, limiting adaptability in dynamic environments and complex mission objectives [10, 11].

Recent advancements in large language models (LLMs) have introduced new opportunities for flexible and generalized reasoning in robotics [12, 13, 14, 15, 16]. Trained on massive text corpora, LLMs demonstrate structured planning, goal inference, and task adaptation across diverse domains

---

\*Corresponding author

<sup>2</sup><https://youtu.be/8zcPYqjWzYo>

<sup>3</sup><https://github.com/ZhouRobotics/LLM-Flock>

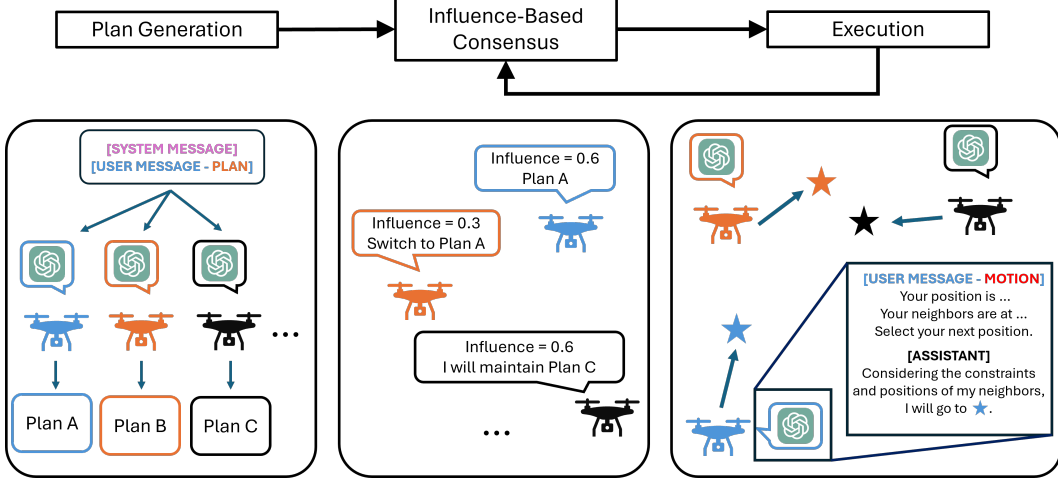


Figure 1: LLM-Flock framework for decentralized multi-robot flocking. Each robot first uses an onboard LLM to generate a candidate plan from a shared prompt. Then robots exchange plans locally and iteratively refine them through an influence-based consensus protocol. Motion execution occurs in parallel, with each robot’s LLM deciding the waypoint location at each step, enabling coordination without centralized control.

without explicit retraining [17, 18]. These capabilities suggest that LLMs could serve as decentralized decision-makers, enabling robots to interpret high-level instructions and generate formation strategies on the fly.

However, directly applying LLMs to decentralized multi-robot coordination presents significant challenges [19, 20, 21]. Independent LLM-driven robots often exhibit hallucinated reasoning, logical inconsistencies, and a lack of collective awareness [22, 23]. Without structured mechanisms to align individual plans, such systems can collapse into degenerate behaviors, such as converging to the centroid or diverging chaotically, undermining effective decentralized control [24, 25].

To address these challenges, we propose *LLM-Flock* (Fig. 1), a decentralized multi-robot flocking framework that integrates LLM-driven local planning with an influence-based consensus protocol. Each robot independently queries an LLM to generate a candidate formation plan based on local objectives and environmental constraints. Robots then iteratively negotiate plan adoption based on the number of neighbors, dynamically driving the team toward coherent and stable formations without centralized coordination or retraining.

The main contributions of this work are:

- We propose a generalizable decentralized framework for multi-robot flocking that combines LLM-based local planning with influence-based consensus.
- We design a structured interaction protocol that unifies decentralized reasoning through lightweight local negotiation.
- We validate the framework across a diverse set of closed-source and open-source LLMs, demonstrating its effectiveness and generality.
- We demonstrate practical feasibility through comprehensive simulations and real-world experiments with physical multi-drone systems.

The remainder of this paper is organized as follows: Section 2 reviews prior work on multi-robot formation control and multi-robot coordination with LLMs. Section 3 details the proposed LLM-Flock framework. Section 4 presents simulation and real-world experiments validating the framework. Section 5 concludes the paper, and Section 6 discusses current limitations and future directions.

## 2 Related Works

**Multi-Robot Formation Control.** Flocking and formation control are well-established topics in multi-robot systems. Classical methods, such as Reynolds’ boid model and Olfati-Saber’s decentralized algorithms, achieve coordination through local rules like separation, alignment, and cohesion [26, 8, 27]. Later studies introduced graph-based consensus protocols to improve stability and scalability [28]. Reinforcement learning (RL) approaches, including MADDPG and QMIX, enable decentralized strategies for multi-robot coordination [29, 30], but typically require extensive training and are sensitive to environment dynamics. Imitation learning such as graph neural networks [31, 32, 33, 34] offers an alternative, but it faces challenges such as dataset dependence and covariate shift.

### LLMs for Multi-Robot Coordination.

LLMs offer new opportunities for flexible reasoning in multi-robot coordination. Recent frameworks such as RoCo [14] and SMART-LLM [35] demonstrate the potential of LLMs for task planning and coordination in multi-robot systems. Other studies, such as ZeroCAP [36], have explored LLM-based formation control, showing promising results. However, these approaches rely on centralized architectures with global environment knowledge, limiting their scalability and real-world applicability.

**Challenges of LLM-Based Decentralized Reasoning.** Despite their promise, LLM-driven robots exhibit hallucinated outputs, logical inconsistencies, and limited awareness of coordination, as noted in [25]. Early attempts of using LLMs for multi-robot flocking show that independently operating LLM-based robots frequently collapse toward a centroid or diverge due to misaligned individual plans, highlighting the need for structured negotiation mechanisms to align decentralized reasoning [24].

**Positioning of This Work.** To address these challenges, we propose LLM-Flock, a framework that integrates LLM-based local planning with an influence-based decentralized consensus protocol. By coupling prompt-driven reasoning with lightweight local negotiation, our approach enables multi-robot teams to dynamically converge toward coherent flocking formations without centralized control or extensive retraining. In contrast to prior work that relies solely on unstructured LLM outputs, LLM-Flock explicitly grounds decentralized coordination by assigning each robot an LLM for plan generation and decision-making through structured, influence-based plan refinement, enabling scalable and robust flocking behaviors.

## 3 Methods

We propose LLM-Flock, a framework for decentralized multi-robot flocking that integrates LLM-driven planning with an influence-based consensus mechanism, as shown in Fig. 1. The framework enables a team of robots to autonomously achieve and maintain a coherent formation without centralized control. Each robot is individually equipped with an LLM that acts as its local planner and decision-maker. The interaction between the robot and its LLM is structured through two types of messages: (i) a one-time plan generation message at the beginning of the mission, and (ii) periodic position update messages during motion execution. The communication of these two types of messages guides the LLM to reason about both the initial formation objective and dynamic local adjustments throughout the mission.

LLM-Flock operates through three key stages: (1) individual plan generation, (2) influence-based, decentralized plan consensus, and (3) coordinated motion execution. The plan generation stage is executed once at mission initialization, while the framework alternates periodically between plan consensus and motion execution thereafter. Each stage is detailed below.

### 3.1 Individual Plan Generation

We consider a team of  $N$  mobile robots, indexed as  $i \in \{1, \dots, N\}$ . Each robot is initialized randomly in the environment at  $\mathbf{x}_i(0) \in \mathbb{R}^2$ . To guide the LLMs during the planning phase, each robot is initialized with a system message that defines the task context, environmental constraints, and

expected behavior. The system message explicitly describes the objective of forming a specified geometric formation, the inter-robot distance requirements, the safe distance constraint, the maximum allowed movement per round, and the communication range. An example system message template is shown below.

**[SYSTEM]** = “ You are a drone navigating in a 2D space. Your objective is to determine your next position to contribute to forming a shape with your neighbors while maintaining specific distance constraints. Your neighbors are also moving.

**Key Requirements:**

Formation: Form a/an  $\{\text{shape}\}$  centered at  $\{\mathbf{x}_c\}$ .

Desired Distance: Maintain a desired distance of  $\{d_d\}$  units between each drone.

Safe Distance: Keep a minimum safe distance of  $\{d_s\}$  units from other drones.

Maximum Speed: Your movement per step cannot exceed  $\{v_m\}$  units.

Communication Range: Your communication range is  $\{r_{comm}\}$  units.

**Task:** Decide your next position considering the above constraints and formation goal. Briefly explain your decision and provide the new position in the format ‘Position:  $[x, y]$ .’ ”

where mission-specific parameters such as desired formation shape, center location  $\mathbf{x}_c \in \mathbb{R}^2$ , desired inter-robot distance  $d_d$ , minimum safe distance between robots  $d_s$ , maximum velocity the robot can move in each round  $v_m$ , and the communication radius for the robot  $r_{comm}$  are dynamically filled based on the task specification.

After receiving the system message, each robot initiates the mission by sending an initial *plan generation user message* to its LLM. This message instructs the LLM to propose a full set of target positions for all robots that satisfy the specified formation constraints. In addition to the overall plan, the LLM is also required to assign the robot’s own role by indicating which specific position it should take within the formation. The plan generation user message template is detailed below.

**[USER]** = “Please make a plan of the locations for the team of  $\{N\}$  robots forming the shape. Remember the given requirements about the shape and desired distance. Please give the final answer in the form of ‘Plan:  $[[x_1, y_1], [x_2, y_2], \dots, [x_n, y_n]]$ ’, and the index of the location you are taking as ‘my plan:  $a$ ’, where  $a$  is the index of the coordinate.”

This message provides the robot with the team size of  $N$  and reiterates the formation requirements to guide the LLM’s reasoning. The LLM is instructed to output a full global plan, denoted as  $\mathcal{P}_i = \{\mathbf{p}_1^i, \mathbf{p}_2^i, \dots, \mathbf{p}_N^i\}$ , where each  $\mathbf{p}_j^i \in \mathbb{R}^2$  specifies the desired position for robot  $j$  according to robot  $i$ ’s local planning. In addition to generating the global plan, the LLM must assign the robot’s own role within the formation by indicating the index of the position it will take, i.e.,  $\mathbf{g}_i = \mathcal{P}_i[a]$ . The output format is explicitly defined to ensure accurate and consistent information extraction across all robots.

After individual plan generation, the system proceeds to the decentralized consensus phase, where robots negotiate and align on a common formation plan.

### 3.2 Influence-based Decentralized Plan Consensus

After the individual plan generation, each robot possesses a locally generated formation plan. However, coherent global formation cannot be achieved if robots pursue conflicting plans. Thus, a decentralized consensus process is necessary to synchronize the team toward a unified plan. To facilitate decentralized negotiation, we introduce the notion of influence, which quantifies a robot’s communication centrality within the network. Intuitively, a robot with more immediate neighbors is considered more influential, as it can propagate its plan more rapidly across the team. The influence from robot  $i$  at time  $t$  is defined as

$$I_i(t) = \frac{|\mathcal{N}_i(t)|}{N}, \quad (1)$$

where  $\mathcal{N}_i(t) = \{j \in \{1, \dots, N\} \setminus \{i\} \mid \|\mathbf{x}_i(t) - \mathbf{x}_j(t)\| \leq r_{comm}\}$  denotes the set of neighboring robots within communication range  $r_{comm}$ , and  $N$  is the total number of robots.

At each consensus round, every robot broadcasts its current formation plan  $\mathcal{P}_i$  and computed influence score  $I_i(t)$  to its neighboring robots  $\mathcal{N}_i(t)$ . Upon receiving plans and influence scores from its neighbors, robot  $i$  identifies the neighbor  $k$  with the highest influence score  $I_k(t)$ . If the neighbor's influence is greater than its own, i.e.,  $I_k(t) > I_i(t)$ , and the neighbor's plan differs from its current plan ( $\mathcal{P}_k \neq \mathcal{P}_i$ ), robot  $i$  adopts the neighbor's plan  $\mathcal{P}_i \leftarrow \mathcal{P}_k$ .

After adopting a new plan, each robot dynamically assigns itself a goal position from the adopted plan based on proximity. Goal assignment is conducted in a decentralized greedy fashion: each robot selects the closest available goal position among the unassigned waypoints in the plan. Once a goal position is assigned to a robot, it becomes unavailable for others. Specifically, robot  $i$  selects its goal  $\mathbf{g}_i$  according to:

$$\mathbf{g}_i = \arg \min_{\mathbf{p} \in \mathcal{P}_i^{\text{avail}}} \|\mathbf{x}_i(t) - \mathbf{p}\|, \quad (2)$$

where  $\mathcal{P}_i^{\text{avail}}$  denotes the set of unassigned goal positions remaining in the plan  $\mathcal{P}_i$ , and  $\mathbf{x}_i(t)$  is the robot's current position. This nearest-available-goal assignment ensures a smooth transition during plan updates, minimizes unnecessary movement, and promotes stability throughout the formation process. If no neighbor possesses a higher influence score, the robot retains its current plan.

This decentralized negotiation process is repeated periodically, with robots dynamically alternating between consensus negotiation and motion execution. Over successive rounds, high-influence plans naturally propagate through the network, enabling the team to progressively refine and converge toward a shared formation plan without requiring global communication or centralized synchronization. The formal influence-based consensus procedure is summarized in Algorithm 1.

---

**Algorithm 1** Influence-Based Plan Consensus

---

```

1: Input: Initial plans  $\mathcal{P}_i$ , neighbor sets  $\mathcal{N}_i(t)$ , and influence scores  $I_i(t)$  for all  $i \in \{1, \dots, N\}$ 
2: Output: Updated formation plans  $\mathcal{P}_i$  and assigned goals  $\mathbf{g}_i$  for all robots
3: for all robot  $i$  in parallel do
4:   Receive  $\mathcal{P}_j$  and  $I_j(t)$  from all  $j \in \mathcal{N}_i(t)$ 
5:    $k \leftarrow \arg \max_{j \in \mathcal{N}_i(t)} I_j(t)$ 
6:   if  $I_k(t) > I_i(t)$  and  $\mathcal{P}_k \neq \mathcal{P}_i$  then
7:      $\mathcal{P}_i \leftarrow \mathcal{P}_k$ 
8:     Initialize available goals:  $\mathcal{P}_i^{\text{avail}} \leftarrow \mathcal{P}_i$ 
9:     Assign goal:  $\mathbf{g}_i \leftarrow \arg \min_{\mathbf{p} \in \mathcal{P}_i^{\text{avail}}} \|\mathbf{x}_i(t) - \mathbf{p}\|$ 
10:    Remove assigned goal from available set:  $\mathcal{P}_i^{\text{avail}} \leftarrow \mathcal{P}_i^{\text{avail}} \setminus \{\mathbf{g}_i\}$ 
11:   end if
12: end for

```

---

Having established the decentralized plan consensus mechanism, we now describe how individual robots execute motion toward their assigned goals.

### 3.3 Motion Execution

Following the influence-based consensus process, each robot proceeds with motion execution while continuously adjusting its trajectory based on local observations. During each update cycle, the robot queries its LLM using a *position update user message* that encodes its current state and nearby environmental information. Specifically, the message includes the robot's current position  $\mathbf{x}_i \in \mathbb{R}^2$ , the set of neighboring robot positions  $\mathcal{X}_i = \{\mathbf{x}_j \mid j \in \mathcal{N}_i(t)\}$ , and its assigned global formation plan  $\mathcal{P}_i$ .

Using this updated local information, the LLM determines the robot's next movement step toward its assigned goal, considering both formation objectives and safety constraints. To ensure robust parsing and minimal ambiguity, the output format is strictly specified. The template for the position update user message is shown below:

**[USER]** = “Current Position:  $\{\mathbf{x}_i\}$ . Moving Neighbor Positions:  $\{\mathcal{X}_i\}$ . Plan:  $\{\mathcal{P}_i\}$ . You will need to go to  $\{\mathbf{g}_i\}$  as your final destination.

**Task:** Decide your next position considering the above constraints and the location of your neighbors. Briefly explain your decision and provide the new position in the format ‘Position:  $[x, y]$ .’ ”

Upon receiving the position update query, the LLM reasons about the robot’s next waypoint  $\mathbf{w}_i(t) \in \mathbb{R}^2$  toward its assigned goal  $\mathbf{g}_i$ , taking into account the updated neighbor configuration and formation constraints.

In summary, LLM-Flock combines local LLM-based planning with an influence-based decentralized consensus mechanism, enabling scalable multi-robot flocking without centralized coordination. Robots autonomously generate individual formation plans, negotiate through local influence-driven interactions, and navigate toward dynamically assigned goal positions. In the following section, we present comprehensive simulations and real-world experiments to evaluate the performance and effectiveness of the proposed framework.

## 4 Results

Our evaluation covers diverse formation tasks, multiple LLM backends, and both simulated environments and real robot experiments. We first present qualitative results illustrating the emergence of flocking behaviors, including a comparison to a baseline without influence-based consensus. We then quantitatively analyze convergence performance across different LLMs and formation shapes. Finally, we validate LLM-Flock’s applicability through real-world experiments with a team of Crazyflie drones [37].

All experiments, unless otherwise specified, use a desired inter-robot distance of 10 units, a maximum speed of 6 units per round, a minimum safe distance of 3 units, and a communication range of 15 units. All the robots are initialized randomly in a 2D environment with 100 by 100 units. Formations are centered at [50, 50], and robots are assumed to have perfect localization in simulation.

### 4.1 Qualitative Simulation Evaluation

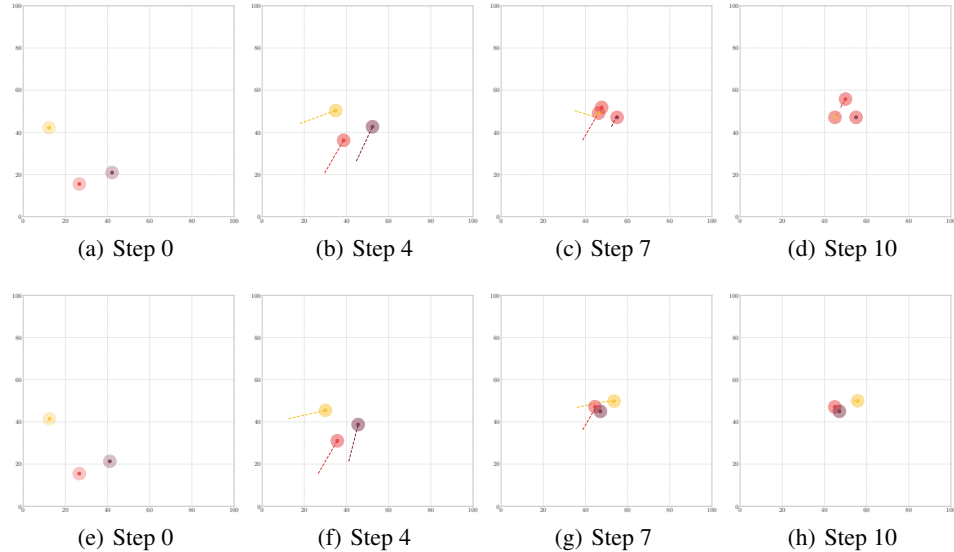


Figure 2: Comparison of formation results with and without influence-based consensus. (a)-(d) show robot trajectories using influence-based plan consensus with three robots forming triangle formations, and (e)-(h) show the trajectories without consensus.

We qualitatively evaluate LLM-Flock by comparing its influence-based consensus approach against a baseline method. Using OpenAI o3-mini as the LLM backend, we test both approaches on triangle

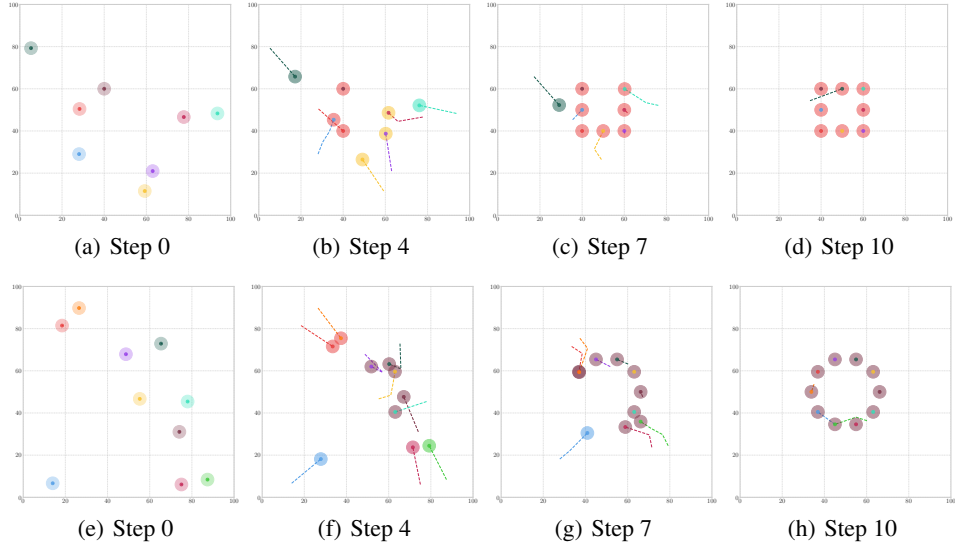


Figure 3: Qualitative results demonstrating LLM-Flock on diverse formation tasks. (a)-(d) show the progression of robot trajectories as eight robots form a square formation using influence-based plan consensus. (e)-(h) show the progression for ten robots forming a circle formation.

formations with three robots. In the baseline, each robot follows its initial plan independently, selecting its assigned goal without negotiating with neighbors. This setup highlights an approach that relies solely on unstructured LLM planning for decentralized formation control.

As shown in Fig. 2, LLM-Flock consistently converges to symmetric triangle formations, with all robots reaching plan consensus by the end of the test. The color of its disk indicates each robot’s identity. Initially, in Fig. 2(a), each robot generates a unique plan, with disk color matching the robot’s identity. In Fig. 2(b), the yellow drone adopts the plan from the red drone due to the higher influence of the red drone, and its disk color switches to red. By the final frame (Fig. 2(d)), all robots share the same plan. In contrast, the baseline results in collapsed or disorganized configurations with inconsistent spacing, as seen in Fig. 2(h). LLM-Flock achieves a well-spaced equilateral triangle, but the baseline frequently produces uneven formations.

To demonstrate the flexibility and scalability of LLM-Flock, we test the framework on a square formation with eight robots and a circle formation with ten robots, as shown in Fig. 3. In both cases, robots successfully arrange themselves along the intended geometric shapes while maintaining the desired inter-robot distance. The square formation yields evenly spaced robots along the edges and corners in Fig. 3(d) and the circle formation achieves smooth alignment around the center at [50, 50] in Fig. 3(h). These results highlight LLM-Flock’s ability to coordinate larger teams and support diverse formation geometries through decentralized influence-based consensus. Additional simulation results are included in the appendix and supplementary materials.

## 4.2 Quantitative Simulation Evaluation

We quantitatively evaluate the convergence performance of LLM-Flock across different language model backends and formation tasks. As a convergence metric, we use the Procrustes shape error [38, 39], which measures the geometric difference between the actual robot formation  $X$  and the target formation  $Y$  after optimal alignment through translation and rotation. Formally, the Procrustes error at timestep  $t$  is computed as:

$$\text{Error}(t) = \frac{1}{N} \sum_{i=1}^N \|\mathbf{x}_i(t) - \mathbf{y}_i\|_2, \quad (3)$$

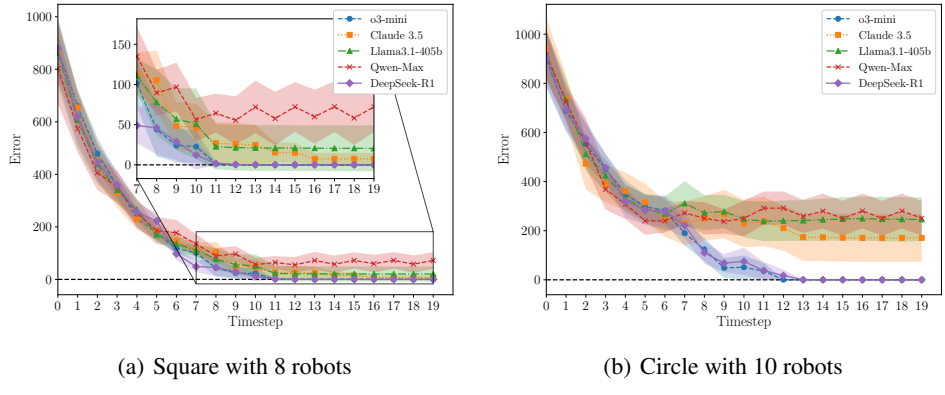


Figure 4: Procrustes shape error over time across different formation tasks and LLM backends. Lines show the mean Procrustes error across 10 randomized trials, with shaded regions representing the 95% confidence intervals.

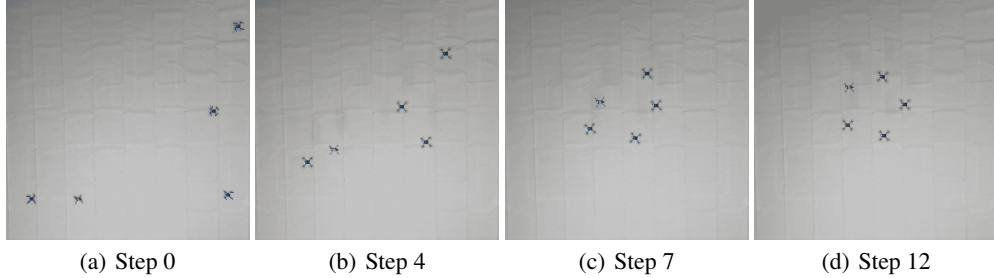


Figure 5: Snapshots of five Crazyflie drones forming a circle using proposed LLM-Flock framework.

where  $\mathbf{x}_i(t)$  and  $\mathbf{y}_i$  denote the aligned positions of robot  $i$  and actual target formation, respectively, and  $N$  is the number of robots. Detailed definitions and approaches for calculating the error can be found in the appendix.

For each configuration, we conduct 10 randomized trials and plot the mean Procrustes error over time, with shaded regions representing the 95% confidence intervals. We use five popular LLMs: OpenAI o3-mini [40], Claude 3.5 Sonnet [41], DeepSeek-R1 [42], Llama3.1-405b [18], and Qwen-Max [43]. Each model is evaluated on triangle formations with three and six robots, a square formation with eight robots, and a circle formation with ten robots. All experiments use the environmental parameters and formation center described earlier. For brevity, we only demonstrate results from square and circular formations. More results are included in Appendix C. Fig. 4 shows that LLM-Flock enables stable convergence across all tested language models and team sizes. Models with stronger reasoning capabilities, such as OpenAI o3-mini and DeepSeek-R1, achieve faster convergence and consistently form the desired formations across all tasks. In contrast, general-purpose models such as Claude 3.5 Sonnet, Qwen-Max, and Llama 3.1 exhibit slower convergence and higher residual errors.

### 4.3 Real Robot Evaluation

We validate the practical feasibility of LLM-Flock using Crazyflie drones in an indoor motion capture environment. Each robot executes the LLM-Flock protocol, performing independent plan generation and influence-based consensus with neighbors using OpenAI o3-mini model. We test a circle formation with five Crazyflie drones initialized from random positions. Snapshots in Fig. 5 show the team progressively converging to a stable circle without centralized control. These results demonstrate that LLM-Flock generalizes beyond simulation to real-world decentralized systems. Additional snapshots are available in Appendix B, and the video is available online<sup>4</sup>.

<sup>4</sup><https://youtu.be/8zcPYqjWzY>

## 5 Conclusion

We introduced LLM-Flock, a decentralized flocking framework that integrates LLM-based local planning with influence-based consensus. The system enables formation control through prompt-driven reasoning and local plan negotiation. Experiments across diverse formations and LLMs, including real-world Crazyflie deployments, show that LLM-Flock achieves stable and scalable flocking without centralized coordination or retraining. By structuring decentralized plan refinement, LLM-Flock mitigates inconsistencies in unstructured LLM reasoning and demonstrates the potential of combining language models with lightweight coordination for multi-robot collaboration.

## 6 Limitations

While LLM-Flock demonstrates effective decentralized flocking across a range of simulated and real-world settings, several limitations remain.

First, a key limitation of LLM-Flock lies in the computational demands of modern language models. Current LLMs are either capable of dealing with complex problems but too large to run on lightweight robot platforms, or they are lightweight but lack sufficient reasoning ability, making on-board inference infeasible. Our real-world experiments rely on external servers to run the models, which requires persistent network connectivity during execution. This reliance restricts deployment in infrastructure-free or communication-limited environments. Enabling local inference through model compression, distillation, or hardware acceleration is an essential step toward the practical and scalable deployment of LLM-based decentralized planning.

Second, although modern LLMs significantly improve structured reasoning, their outputs remain susceptible to inconsistencies, particularly under partial or ambiguous observations of neighboring states. Since each robot reasons independently based on local perceptions and prompts, small errors or misinterpretations may propagate before consensus corrects them. Enhancing robustness through local verification mechanisms, feedback loops, or multi-step reasoning chains remains an open area for exploration.

Third, the overall performance of LLM-Flock inherently depends on the zero-shot planning accuracy of the underlying language model. Quantitative experiments show that stronger reasoning models, such as DeepSeek-R1 and o3-mini, converge more rapidly and achieve lower residual errors than more general-purpose LLMs like Claude 3.5 Sonnet or Qwen-Max. Improving reasoning ability and output accuracy remains an important direction for future work.

Finally, while current formation tasks focus on relatively simple geometric shapes, scaling the framework to more complex, dynamic, or mission-driven formations presents additional challenges. Future work includes developing hierarchical planning strategies where LLMs reason about both formation structure and dynamic adaptation to evolving objectives.

## References

- [1] L. Shijie, S. Yefeng, G. Liang, and Z. Kai. Trajectory tracking method of agricultural machinery multi-robot formation operation based on mpc delay compensator. *Smart Agriculture*, 6(3):69, 2024.
- [2] L. Peng, F. Guan, L. Perneel, H. Fayyad-Kazan, and M. Timmerman. Decentralized multi-robot formation control with communication delay and asynchronous clock. *Journal of Intelligent & Robotic Systems*, 89:465–484, 2018.
- [3] R. Konda, H. M. La, and J. Zhang. Decentralized function approximated q-learning in multi-robot systems for predator avoidance. *IEEE Robotics and Automation Letters*, 5(4):6342–6349, 2020.
- [4] N. Bouraqadi, A. Doniec, and E. de Douai. Flocking-based multi-robot exploration. In *National conference on control architectures of robots*, pages 23–24, 2009.
- [5] G. Notomista, C. Pacchierotti, and P. R. Giordano. Multi-robot persistent environmental monitoring based on constraint-driven execution of learned robot tasks. In *2022 International Conference on Robotics and Automation (ICRA)*, pages 6853–6859. IEEE, 2022.
- [6] K.-C. Ma, Z. Ma, L. Liu, and G. S. Sukhatme. Multi-robot informative and adaptive planning for persistent environmental monitoring. In *Distributed Autonomous Robotic Systems: The 13th International Symposium*, pages 285–298. Springer, 2018.
- [7] W. Burgard, M. Moors, C. Stachniss, and F. E. Schneider. Coordinated multi-robot exploration. *IEEE Transactions on robotics*, 21(3):376–386, 2005.
- [8] R. Olfati-Saber. Flocking for multi-agent dynamic systems: Algorithms and theory. *IEEE Transactions on automatic control*, 51(3):401–420, 2006.
- [9] S. Shao, J. Zhang, T. Wang, A. Shankar, and C. Maple. Dynamic obstacle-avoidance algorithm for multi-robot flocking based on improved artificial potential field. *IEEE Transactions on Consumer Electronics*, 70(1):4388–4399, 2023.
- [10] M. De Denus, J. Anderson, and J. Baltes. Heuristic formation control in multi-robot systems using local communication and limited identification. In *RoboCup 2009: Robot Soccer World Cup XIII 13*, pages 437–448. Springer, 2010.
- [11] G. Antonelli, F. Arrichiello, F. Caccavale, and A. Marino. Decentralized time-varying formation control for multi-robot systems. *The International Journal of Robotics Research*, 33(7):1029–1043, 2014.
- [12] Z. Tao, T.-E. Lin, X. Chen, H. Li, Y. Wu, Y. Li, Z. Jin, F. Huang, D. Tao, and J. Zhou. A survey on self-evolution of large language models. *arXiv preprint arXiv:2404.14387*, 2024.
- [13] P. Li, Z. An, S. Abrar, and L. Zhou. Large language models for multi-robot systems: A survey. *arXiv preprint arXiv:2502.03814*, 2025.
- [14] Z. Mandi, S. Jain, and S. Song. Roco: Dialectic multi-robot collaboration with large language models. In *2024 IEEE International Conference on Robotics and Automation (ICRA)*, pages 286–299. IEEE, 2024.
- [15] Y. Wang, R. Xiao, J. Y. L. Kasahara, R. Yajima, K. Nagatani, A. Yamashita, and H. Asama. Dart-llm: Dependency-aware multi-robot task decomposition and execution using large language models. *arXiv preprint arXiv:2411.09022*, 2024.
- [16] Y. Wu, Y. Tao, P. Li, G. Shi, G. S. Sukhatmem, V. Kumar, and L. Zhou. Hierarchical LLMs In-the-loop Optimization for Real-time Multi-Robot Target Tracking under Unknown Hazards, Sept. 2024. URL <http://arxiv.org/abs/2409.12274>. arXiv:2409.12274.

- [17] J. Achiam, S. Adler, S. Agarwal, L. Ahmad, I. Akkaya, F. L. Aleman, D. Almeida, J. Altenschmidt, S. Altman, S. Anadkat, et al. Gpt-4 technical report. *arXiv preprint arXiv:2303.08774*, 2023.
- [18] A. Grattafiori, A. Dubey, A. Jauhri, A. Pandey, A. Kadian, A. Al-Dahle, A. Letman, A. Mathur, A. Schelten, A. Vaughan, et al. The llama 3 herd of models. *arXiv preprint arXiv:2407.21783*, 2024.
- [19] W. Hunt, S. D. Ramchurn, and M. D. Soorati. A Survey of Language-Based Communication in Robotics. *arXiv preprint arXiv:2406.04086*, Sept. 2024. doi:10.48550/arXiv.2406.04086. URL <http://arxiv.org/abs/2406.04086>.
- [20] Y. Kim, D. Kim, J. Choi, J. Park, N. Oh, and D. Park. A Survey on Integration of Large Language Models with Intelligent Robots. *arXiv preprint arXiv:2404.09228*, Aug. 2024. doi:10.48550/arXiv.2404.09228. URL <http://arxiv.org/abs/2404.09228>.
- [21] T. Guo, X. Chen, Y. Wang, R. Chang, S. Pei, N. V. Chawla, O. Wiest, and X. Zhang. Large Language Model based Multi-Agents: A Survey of Progress and Challenges. *arXiv preprint arXiv:2402.01680*, Apr. 2024. doi:10.48550/arXiv.2402.01680. URL <http://arxiv.org/abs/2402.01680>.
- [22] L. Huang, W. Yu, W. Ma, W. Zhong, Z. Feng, H. Wang, Q. Chen, W. Peng, X. Feng, B. Qin, et al. A survey on hallucination in large language models: Principles, taxonomy, challenges, and open questions. *ACM Transactions on Information Systems*, 2023.
- [23] D. McDonald, R. Papadopoulos, and L. Benningfield. Reducing llm hallucination using knowledge distillation: A case study with mistral large and mmlu benchmark. *Authorea Preprints*, 2024.
- [24] P. Li, V. Menon, B. Gudiguntha, D. Ting, and L. Zhou. Challenges faced by large language models in solving multi-agent flocking. *arXiv preprint arXiv:2404.04752*, 2024.
- [25] W. Chen, S. Koenig, and B. Dilkina. Why solving multi-agent path finding with large language model has not succeeded yet. *arXiv preprint arXiv:2401.03630*, 2024.
- [26] C. W. Reynolds. Flocks, herds and schools: A distributed behavioral model. In *Proceedings of the 14th annual conference on Computer graphics and interactive techniques*, pages 25–34, 1987.
- [27] J. Blumenkamp, S. Morad, J. Gielis, Q. Li, and A. Prorok. A framework for real-world multi-robot systems running decentralized gnn-based policies. In *2022 International Conference on Robotics and Automation (ICRA)*, pages 8772–8778. IEEE, 2022.
- [28] M. Goarin and G. Loianno. Graph neural network for decentralized multi-robot goal assignment. *IEEE Robotics and Automation Letters*, 2024.
- [29] R. Lowe, Y. I. Wu, A. Tamar, J. Harb, O. Pieter Abbeel, and I. Mordatch. Multi-agent actor-critic for mixed cooperative-competitive environments. *Advances in neural information processing systems*, 30, 2017.
- [30] T. Rashid, M. Samvelyan, C. S. De Witt, G. Farquhar, J. Foerster, and S. Whiteson. Monotonic value function factorisation for deep multi-agent reinforcement learning. *Journal of Machine Learning Research*, 21(178):1–51, 2020.
- [31] S. Chen, Y. Sun, P. Li, L. Zhou, and C.-T. Lu. Spatial temporal graph neural networks for decentralized control of robot swarms. In *Proceedings of the 31st ACM International Conference on Advances in Geographic Information Systems*, pages 1–4, 2023.

- [32] S. Chen, Y. Sun, P. Li, L. Zhou, and C.-T. Lu. Learning decentralized flocking controllers with spatio-temporal graph neural network. In *2024 IEEE International Conference on Robotics and Automation (ICRA)*, pages 2596–2602. IEEE, 2024.
- [33] E. Tolstaya, F. Gama, J. Paulos, G. Pappas, V. Kumar, and A. Ribeiro. Learning decentralized controllers for robot swarms with graph neural networks. In *Conference on robot learning*, pages 671–682. PMLR, 2020.
- [34] A. Khan, E. Tolstaya, A. Ribeiro, and V. Kumar. Graph policy gradients for large scale robot control. In *Conference on robot learning*, pages 823–834. PMLR, 2020.
- [35] S. S. Kannan, V. L. Venkatesh, and B.-C. Min. Smart-llm: Smart multi-agent robot task planning using large language models. In *2024 IEEE/RSJ International Conference on Intelligent Robots and Systems (IROS)*, pages 12140–12147. IEEE, 2024.
- [36] V. L. N. Venkatesh and B.-C. Min. ZeroCAP: Zero-Shot Multi-Robot Context Aware Pattern Formation via Large Language Models, Sept. 2024. URL <http://arxiv.org/abs/2404.02318>. arXiv:2404.02318.
- [37] Bitcraze crazyflie. <https://www.bitcraze.io/>. Accessed: 2025-04-15.
- [38] J. C. Gower and G. B. Dijksterhuis. *Procrustes problems*, volume 30. Oxford University Press, USA, 2004.
- [39] D. G. Kendall. A survey of the statistical theory of shape. *Statistical Science*, 4(2):87–99, 1989.
- [40] OpenAI. Openai o3-mini, January 2025. URL <https://openai.com/index/openai-o3-mini/>. Accessed April 30, 2025.
- [41] Anthropic. Claude 3.5 sonnet, October 2024. URL <https://www.anthropic.com/news/clause-3-5-sonnet>. Accessed April 30, 2025.
- [42] D. Guo, D. Yang, H. Zhang, J. Song, R. Zhang, R. Xu, Q. Zhu, S. Ma, P. Wang, X. Bi, et al. Deepseek-r1: Incentivizing reasoning capability in llms via reinforcement learning. *arXiv preprint arXiv:2501.12948*, 2025.
- [43] A. Yang, B. Yang, B. Zhang, B. Hui, B. Zheng, B. Yu, C. Li, D. Liu, F. Huang, H. Wei, et al. Qwen2. 5 technical report. *arXiv preprint arXiv:2412.15115*, 2024.

## A LLM Prompting Details

To illustrate how robots in LLM-Flock interact with language models during decentralized formation, we present a representative simulation in which three robots are tasked with forming an equilateral triangle centered at [50, 50]. Each robot is equipped with its own instance of an LLM (OpenAI o3-mini), serving as its local planner and decision-maker. The mission specifies a desired inter-robot distance of 10 units, a maximum movement speed of 6 units per round, and a communication range of 15 units. This simple example is chosen for clarity, but the same prompt-driven interaction and influence-based consensus process generalize naturally to larger and more complex formations due to the decentralized structure of the framework.

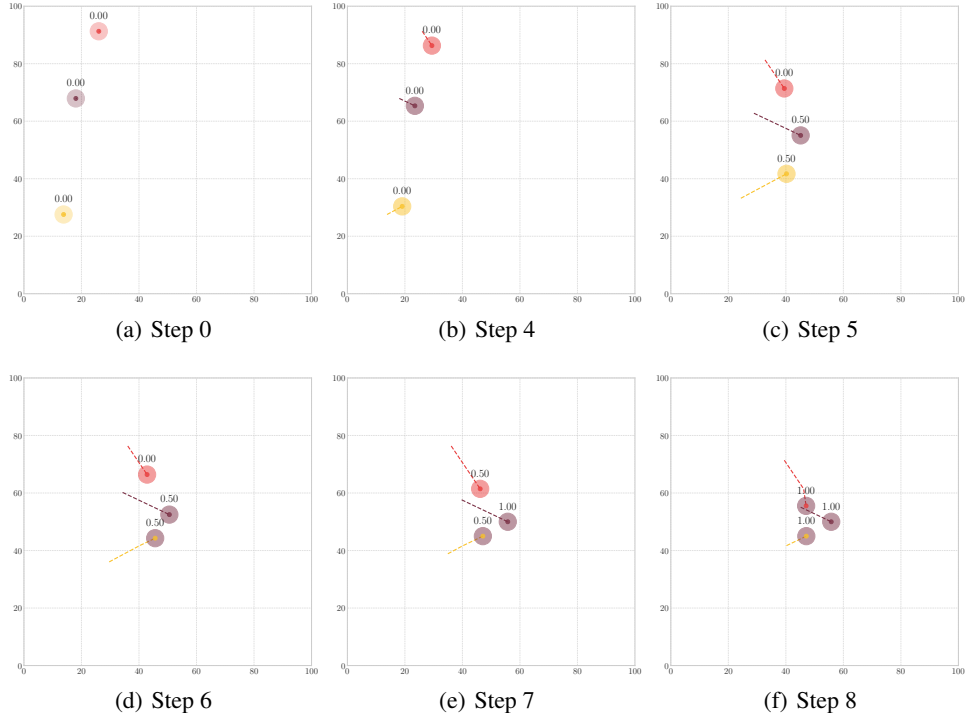


Figure 6: Snapshots of simulation with three robots forming an equilateral triangle. The number on top of the robot demonstrates the influence of the robot. (a) shows the initial positions of the robots. (b) shows the motion execution based on the decision made by individual LLMs. (c)-(f) shows the process of the influence-based consensus with the plan unified at the end of the simulation among all three robots.

The snapshots of this simulation are shown in Fig. 6. Here, we focus on the brown robot. The blue text box below shows the inputs to the LLM, and the brown text box shows the output from the LLM for the brown robot.

### A.1 System Prompt

In the first round, the LLM receives the system prompt, which defines the role of the LLM and the requirements for the brown robot.

**[SYSTEM]** = “You are a drone navigating in a 2D space. Your objective is to determine your next position to contribute to forming a shape with your neighbors while maintaining specific distance constraints. Your neighbors are moving like you.

**Key Requirements:**

Formation: Form an equilateral triangle centering at [50, 50].

Desired Distance: Maintain a desired distance of 10 units between each drone.

Safe Distance: Keep a minimum safe distance of 3 units from other drones.

Maximum Speed: Your movement per step cannot exceed 6 units.

**Task:**

Decide your next position considering the above constraints and formation goal. Briefly explain your decision and provide the new position in the format ‘Position:[x, y].’”

## A.2 User Prompt - Plan Generation

The following message was sent to the LLM inquiring a plan:

**[USER]** = “Please make a plan of the locations for the team of 3 robots forming a/an equilateral triangle with desired distance between robots to be 10.

Please give the final answer in the form of ‘Plan: [[x\_1, y\_1], [x\_2, y\_2], …, [x\_n, y\_n]]’, and the index of the location you are taking as ‘my\_plan: a’, where a is the index of your assigned coordinate.”

The LLM responds with a generated plan:

**[ASSISTANT]** = “ To achieve an equilateral triangle formation centered at [50, 50] with a side length of 10 units, we can determine the triangle’s vertices relative to the centroid. In an equilateral triangle, the distance from the centroid to any vertex is given by  $\frac{\sqrt{3}}{3} \cdot \text{side}$ . For a side length of 10, that distance is approximately 5.7735 units.

Using this distance, we can compute the three vertices at the following angular directions:

- **Vertex 0** ( $0^\circ$  to the right):

$$[50 + 5.7735, 50] \approx [55.77, 50]$$

- **Vertex 1** ( $120^\circ$ ):

$$\begin{aligned} & [50 + 5.7735 \cdot \cos(120^\circ), 50 + 5.7735 \cdot \sin(120^\circ)] \\ &= [50 - 2.88675, 50 + 5.0] = [47.11, 55] \end{aligned}$$

- **Vertex 2** ( $240^\circ$ ):

$$\begin{aligned} & [50 + 5.7735 \cdot \cos(240^\circ), 50 + 5.7735 \cdot \sin(240^\circ)] \\ &= [50 - 2.88675, 50 - 5.0] = [47.11, 45] \end{aligned}$$

These vertices ensure that:

- The triangle is equilateral (each side is 10 units),
- The centroid is located at [50, 50],
- The robots are spaced according to the desired distance.

Since my index is 0, I will take the coordinate corresponding to Vertex 0.

Plan: [[55.77, 50], [47.11, 55], [47.11, 45]]

my\_plan: 0

From this response, the robot extracts:

- The full plan:  $\mathcal{P}_i = \{[55.77, 50.0], [47.11, 56], [47.11, 45]\}$
- Its assigned goal:  $\mathbf{g}_i = \mathbf{p}_0^i = [55.77, 50.0]$

The plan and index are parsed via regular expressions and validated before proceeding to the consensus stage. Other robots follow similar procedures using their local prompts and positions, resulting in multiple candidate plans to be resolved through influence-based consensus, as shown in Fig. 6(c)-6(f).

### A.3 User Prompt - Motion Execution

After selecting its assigned goal position from either the original plan or consensus plan, each robot proceeds with local motion execution. In each round, the robot sends a *position update* message to its LLM, providing the current state, nearby neighbor positions, and formation goal. Below is an example query and the corresponding LLM response from brown robot in the triangle example.

**[USER] = “Current Positions:**  
 Your Location: [12.63, 70.48]  
 Moving Neighbor Locations: [[22.67, 96.23], [8.52, 24.74]]

**Task:** Decide your next position considering the above constraints and formation goal. Briefly explain your decision and provide the new position in the format "Position: [x, y]"."

The LLM for the brown robot makes a decision on the next step of motion execution as follows:

**[ASSISTANT] =** “I’m currently at [12.63, 70.48] with my target being [55.77, 50]. The straight-line vector from my position to the target is (43.14, -20.48) with an approximate distance of 47.75 units. Since I can only move up to 6 units per step, I calculate a proportional move along that direction.

- **Step 1:** Calculate the unit vector:

$$\text{Unit vector} \approx \left( \frac{43.14}{47.75}, \frac{-20.48}{47.75} \right) \approx (0.903, -0.429)$$

- **Step 2:** Multiply by the max step of 6:

$$\text{Movement} \approx (6 \times 0.903, 6 \times -0.429) \approx (5.42, -2.57)$$

- **Step 3:** Compute new position:

$$\text{New position} \approx [12.63 + 5.42, 70.48 - 2.57] = [18.05, 67.91]$$

Before moving, I verified that I am keeping a safe distance (minimum 3 units) from moving neighbors. With neighbor positions [22.67, 96.23] and [8.52, 24.74], this new position maintains a generous clearance.

**Position:** [18.05, 67.91]”

The robot extracts the motion execution and moves to the next position, as shown in Fig. 6(b)

## B Additional Results

In this section, we present additional results both in simulation and real robot experiments.

### B.1 Qualitative Simulation Results

We evaluate the qualitative behavior of LLM-Flock across four formation tasks using OpenAI o3-mini as the LLM backend. Each task is tested both with and without the proposed influence-based plan consensus mechanism. The tests include triangle formations with three (Fig. 7) and six (Fig. 8)

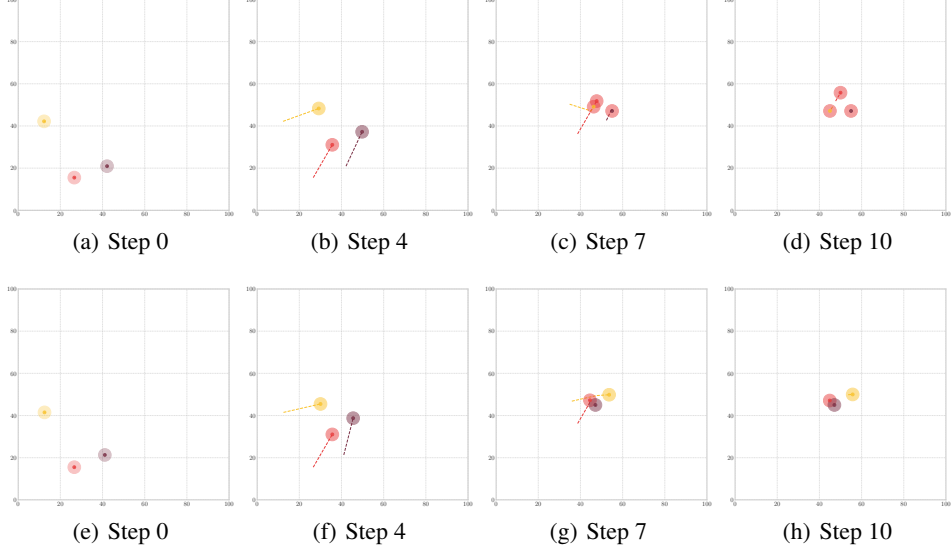


Figure 7: Three robots forming a triangle using OpenAI o3-mini. (a)–(d): With influence-based consensus, robots successfully converge to an equilateral triangle with unified plan alignment. (e)–(h): Without consensus, robots follow conflicting plans, leading to disorganized final positions.

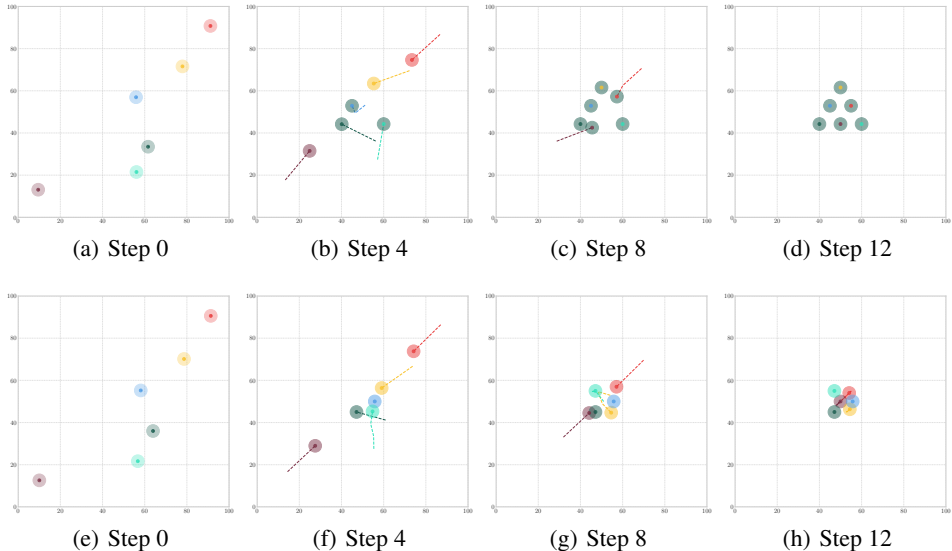


Figure 8: Six robots forming a triangle using OpenAI o3-mini. (a)–(d): LLM-Flock enables convergence to a large equilateral triangle with consistent spacing. (e)–(h): Without influence-based plan consensus, robots exhibit misaligned spacing and failure to form the intended structure.

robots, a square with eight robots (Fig. 9), and a circle with ten robots (Fig. 10). Robots are initialized from random positions in each run. The goal is to assess whether the team can self-organize into the desired geometric formation through decentralized planning and local negotiation.

## B.2 Extended Simulation Quantitative Results

To further evaluate the effectiveness and generalizability of LLM-Flock, we conduct extensive simulation trials across multiple formation geometries and language model backends. Specifically, we measure the shape accuracy over time using the Procrustes error metric, which quantifies deviation from the ideal formation up to rigid-body transformations and is formulated in Appendix C. For

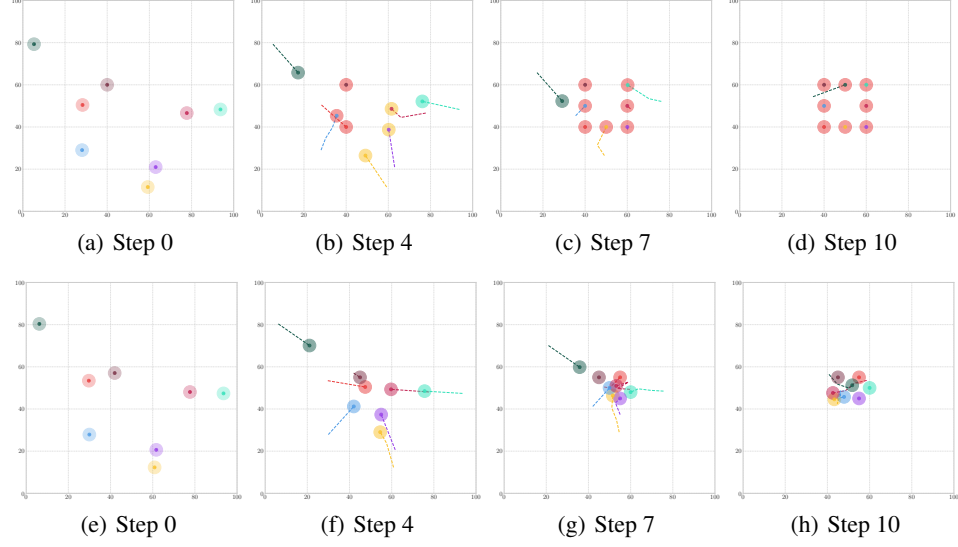


Figure 9: Eight robots forming a square. (a)–(d): Influence-based plan consensus leads to uniform distribution along the square boundary. (e)–(h): Baseline planning without consensus yields scattered and misaligned placements.

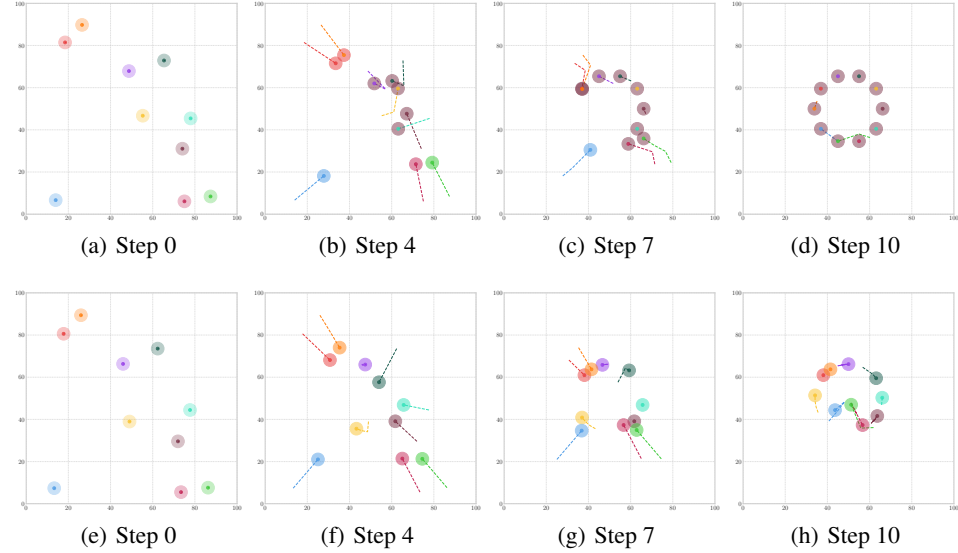


Figure 10: Ten robots forming a circle. (a)–(d): Robots converge to evenly spaced positions around the circular boundary using LLM-Flock. (e)–(h): Without consensus, inconsistent goal assignments lead to disorganized structures.

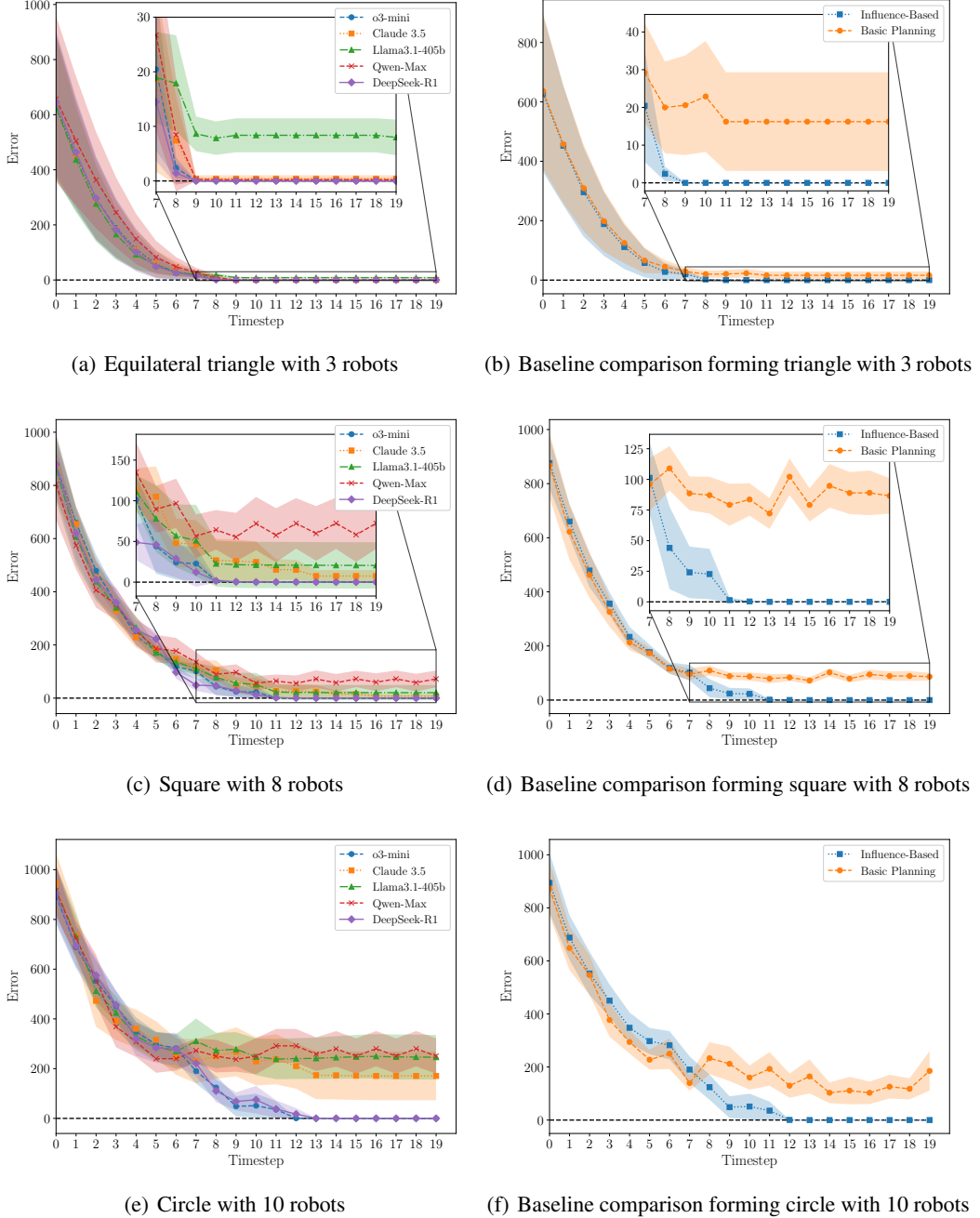


Figure 11: Procrustes shape error over time across different formation tasks and LLM backends. Left column ((a), (c), (e)) shows average Procrustes error across 10 randomized trials using different LLMs under the proposed influence-based consensus framework. Right column ((b), (d), (f)) compares performance with and without consensus using o3-mini. Shaded regions represent 95% confidence intervals. Results demonstrate that influence-based consensus significantly improves formation stability and consistency.

each tested configuration, we perform 10 randomized trials and compute the mean Procrustes error at each timestep, along with 95% confidence intervals.

Figure 11 (left column) presents results for triangle (3-robot), square (8-robot), and circle (10-robot) formations under the influence-based consensus protocol using five popular LLMs: o3-mini, Claude

3.5 Sonnet, DeepSeek-R1, Llama3.1-405b, and Qwen-max. Strong reasoning models such as o3-mini and DeepSeek-R1 consistently achieve low error and fast convergence, demonstrating robust shape formation across team sizes. General-purpose LLMs exhibit higher error and slower stabilization but still improve over time under our consensus framework.

To highlight the importance of influence-based negotiation, we also include comparisons against a baseline setting in which each robot follows its initial LLM-generated plan independently, without plan consensus. As shown in the right column of Fig. 11, baseline trials yield significantly higher Procrustes error and greater variance, especially in larger formations. These results emphasize that LLM-Flock’s structured plan consensus mechanism is critical for achieving coherent decentralized formations, even when using high-performing LLMs.

### B.3 Real Robot Experiment

To further validate the real-world applicability of LLM-Flock, we conducted four physical experiments using Crazyflie drones with increasing team sizes. As shown in Fig. 12, the tested formations include a triangle with three drones, a square with four drones, a cross with five drones, and a circle with five drones. These experiments demonstrate that the proposed framework scales effectively across varying team sizes and geometries while achieving desired formations through decentralized coordination in real environments.

## C Procrustes Error

To quantitatively evaluate the accuracy of multi-robot formations, we adopt the *Procrustes error* as a shape comparison metric. This error measures how closely one set of points (e.g., robot positions) matches another (e.g., an ideal formation) after removing differences in global position and orientation. In our context, it objectively evaluates whether the final robot positions form the desired geometric shape, independent of absolute orientation or location.

The Procrustes error is particularly well suited for this task because:

- It captures shape similarity between two configurations, ignoring irrelevant differences such as global translation or rotation.
- It is sensitive to geometric distortion, effectively detecting irregular formations.
- It enables consistent quantitative comparisons across different team sizes and formation types.

Let the actual team configuration be:

$$X = [\mathbf{x}_1 \quad \mathbf{x}_2 \quad \cdots \quad \mathbf{x}_N] \in \mathbb{R}^{2 \times N},$$

and the target (ideal) configuration be:

$$Y = [\mathbf{y}_1 \quad \mathbf{y}_2 \quad \cdots \quad \mathbf{y}_N] \in \mathbb{R}^{2 \times N},$$

where each  $\mathbf{x}_i, \mathbf{y}_i \in \mathbb{R}^2$  is the 2D position of robot  $i$ .

### Step 1: Remove Translation

Compute the centroids of both sets:

$$\bar{\mathbf{x}} = \frac{1}{N} \sum_{i=1}^N \mathbf{x}_i, \quad \bar{\mathbf{y}} = \frac{1}{N} \sum_{i=1}^N \mathbf{y}_i.$$

Center the shapes:

$$\tilde{X} = X - \bar{\mathbf{x}}\mathbf{1}^\top, \quad \tilde{Y} = Y - \bar{\mathbf{y}}\mathbf{1}^\top$$

where  $\mathbf{1} \in \mathbb{R}^N$  is a vector of ones.

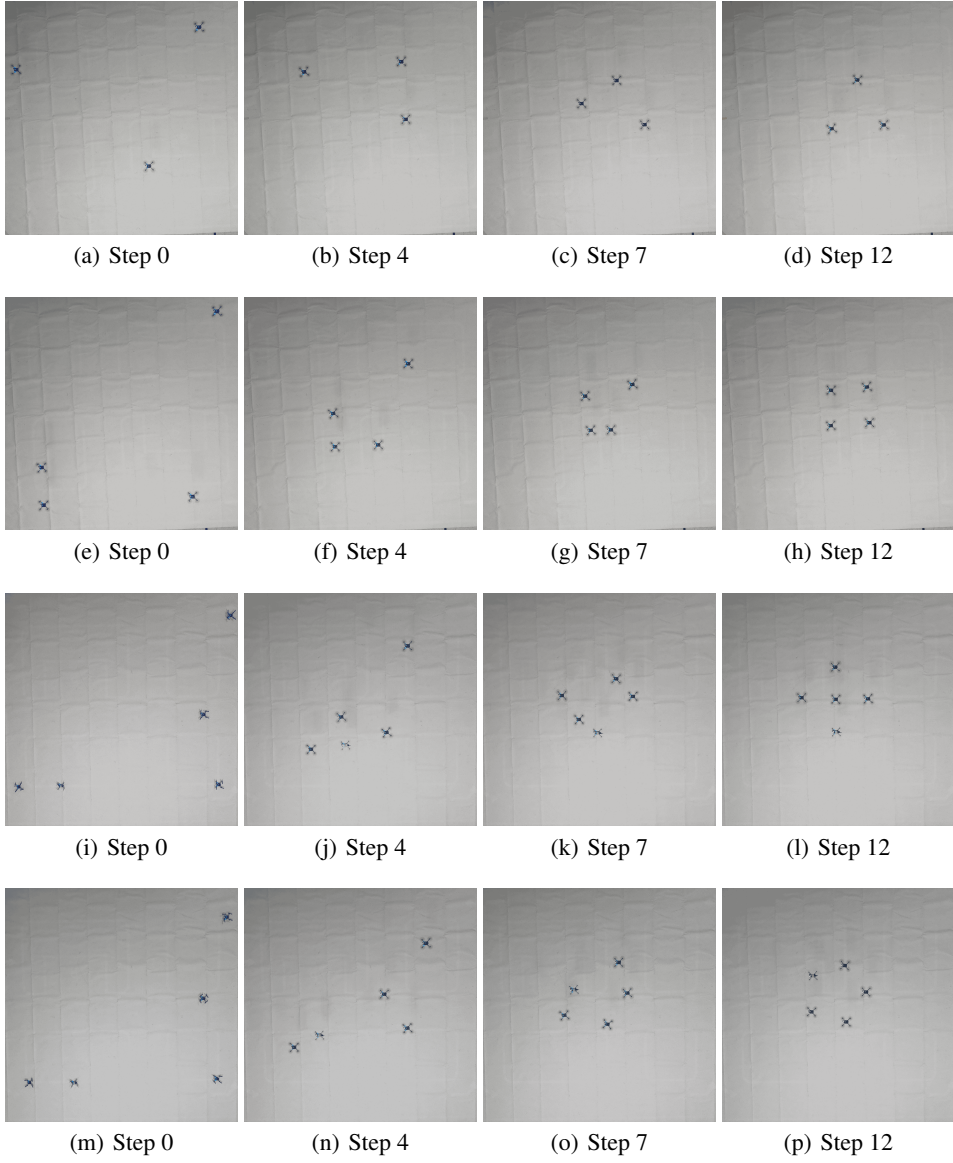


Figure 12: Real drone experiments using proposed LLM-Flock framework with o3-mini as LLM backend. (a)–(d): Forming a triangle with three drones. (e)–(h): Forming a square with four drones. (i)–(l): Forming a cross with five drones. (m)–(p): Forming a circle with five drones.

### Step 2: Optimal Rotation Alignment

We seek the optimal rotation matrix  $R \in \text{SO}(2)$  that minimizes the squared Frobenius norm:

$$R^* = \arg \min_{R \in \text{SO}(2)} \|R\tilde{X} - \tilde{Y}\|_F^2.$$

This is solved via the Singular Value Decomposition (SVD) of the cross-covariance matrix:

$$M = \tilde{Y}\tilde{X}^\top = U\Sigma V^\top.$$

Then the optimal rotation is:

$$R^* = UV^\top.$$

If  $\det(R^*) = -1$ , the solution involves reflection. In that case, the sign of the last singular value in  $\Sigma$  is flipped to enforce a proper rotation.

### Step 3: Compute Procrustes Error

The aligned version of the shape is:

$$\hat{X} = R^*\tilde{X}.$$

The Procrustes error is then given by:

$$E_{\text{proc}} = \frac{1}{N} \|\hat{X} - \tilde{Y}\|_F^2 = \frac{1}{N} \sum_{i=1}^N \|R^*(\mathbf{x}_i - \bar{\mathbf{x}}) - (\mathbf{y}_i - \bar{\mathbf{y}})\|^2.$$

This metric is:

- **Translation invariant** — both sets are centered before alignment.
- **Rotation invariant** — optimal  $R^*$  minimizes misalignment.

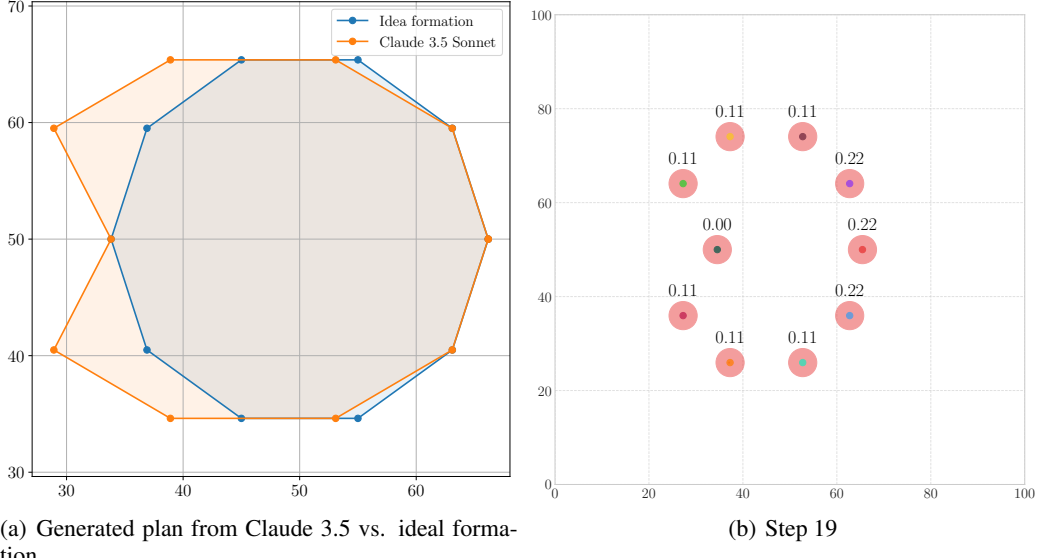
## D Failure Analysis

While LLM-Flock consistently enables stable and coherent formations across a range of shapes, failures can still occur when the LLM generates incorrect outputs, as illustrated by the quantitative results in Fig. 11. In this section, we highlight two representative failure cases that demonstrate how LLM-generated mistakes can impact system behavior: (1) incorrect plan generation, where the proposed formation geometry is invalid or poorly structured, and (2) flawed motion execution, where the generated actions violate the intended trajectory or fail to converge.

### D.1 Incorrect Plan Generation

We assess the failure caused by incorrect geometric reasoning of LLMs. A robot equipped with Claude 3.5 Sonnet is tasked to generate a formation plan for ten robots arranged in a circle centered at [50, 50], with a desired inter-robot spacing of 10 units. As shown in Fig. 13(a), Claude 3.5 Sonnet produces a set of points that deviate significantly from the intended circular shape, with uneven spacing and noticeable distortion compared to the ideal team formation. This faulty plan ends up propagating to the entire team, and the final formation does not represent an ideal uniformly spaced circular shape as shown in Fig. 13(b).

These results reinforce the importance of the strong reasoning capability of the LLMs for decentralized planning. However, as our previous quantitative results Fig 10(e) - 10(h) show, models with strong reasoning ability (e.g., o3-mini) are still insufficient to reliably achieve coherent multi-robot formation alone without our proposed plan consensus framework.



(a) Generated plan from Claude 3.5 vs. ideal formation

(b) Step 19

Figure 13: Comparison of formation plans generated by Claude 3.5 Sonnet and ideal formation for a 10-robot circle formation centered at [50, 50]. (a) Claude 3.5 generates irregular positions that break the intended shape. (b) The distorted plan propagates to the entire team and leads to a failed formation.

## D.2 Incorrect Motion Execution

While LLM-Flock demonstrates consistent convergence in most scenarios, execution stability can be impacted by incorrect motion planning decisions from the LLMs. Fig. 14 shows a failure case in a three-robot triangle formation task using Qwen-Max as the LLM backend. Although all robots successfully reach a consensus on a common plan, one robot (in red) exhibits unstable execution behavior. The behavior of the red robot in Fig. 14(a) is shown below.

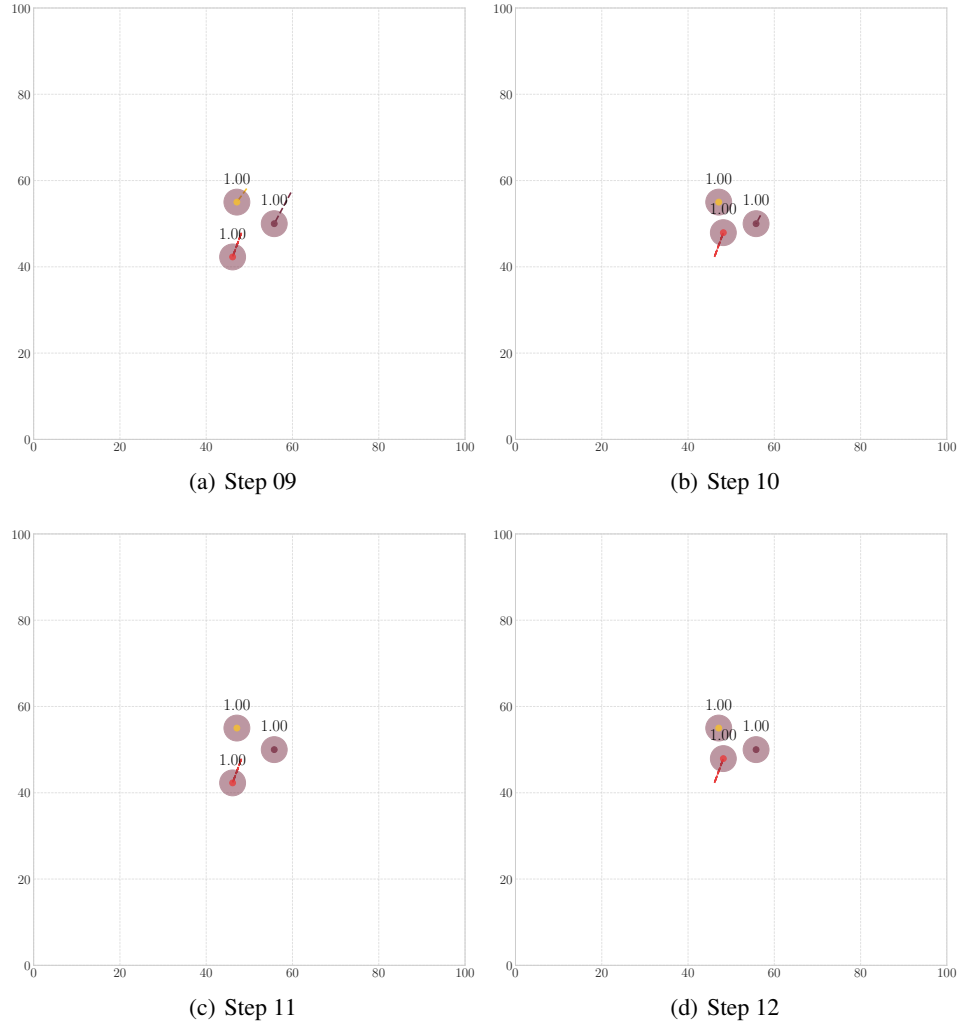


Figure 14: Snapshots from a simulation in which the LLM fails to execute correct motion behavior. In this example, three robots use Qwen-Max to form an equilateral triangle. The red robot consistently applies maximum velocity during execution, causing it to overshoot the goal position and oscillate without stabilizing.

**[ASSISTANT]** = “ To illustrate the LLM’s reasoning process during motion execution, we present a sample step-by-step decision trace. In this scenario, a robot aims to move toward its assigned goal while considering neighbor positions and physical constraints.

**Current Situation:**

- Current position: [46.12, 42.29]
- Neighboring robot positions: [[56.8, 51.93], [47.11, 55.0]]
- Assigned goal position: [47.11, 45]

**Constraints:**

- Desired distance: 10 units
- Safe distance: 3 units
- Maximum speed per round: 6 units

**Step 1: Compute Direction Vector**

$$\text{Direction Vector} = [47.11 - 46.12, 45 - 42.29] = [0.99, 2.71]$$

**Step 2: Normalize the Direction Vector**

$$\|\text{Direction Vector}\| = \sqrt{0.99^2 + 2.71^2} = \sqrt{0.98 + 7.34} = \sqrt{8.32} \approx 2.88$$

$$\text{Unit Vector} = \left[ \frac{0.99}{2.88}, \frac{2.71}{2.88} \right] \approx [0.344, 0.939]$$

**Step 3: Scale by Maximum Speed**

$$\text{Movement Vector} = 6 \cdot [0.344, 0.939] \approx [2.06, 5.63]$$

$$\text{Next Position} = [46.12 + 2.06, 42.29 + 5.63] = [48.18, 47.92]$$

**Step 4: Constraint Validation**

- Distance to [56.8, 51.93]:

$$\sqrt{(56.8 - 48.18)^2 + (51.93 - 47.92)^2} \approx \sqrt{74.30 + 16.08} = \sqrt{90.38} \approx 9.51$$

- Distance to [47.11, 55.0]:

$$\sqrt{(47.11 - 48.18)^2 + (55.0 - 47.92)^2} \approx \sqrt{1.14 + 50.13} = \sqrt{51.27} \approx 7.16$$

- Movement magnitude:

$$\sqrt{2.06^2 + 5.63^2} = \sqrt{4.24 + 31.69} = \sqrt{35.93} \approx 6.0$$

All constraints are satisfied.

**Final Decision:**

Position: [48.18, 47.92]

”

Despite computing a distance of only 2.88 units to the target in **Step 2**, which is below the maximum speed limit of 6 units, the robot still executes a full-speed move. As shown in Fig. 14(a)–14(d), the red robot repeatedly overshoots its goal by applying maximum velocity in every step, leading to oscillatory behavior and failure to converge within the desired tolerance. This behavior stems from the LLM’s flawed numerical reasoning or misinterpretation of geometric constraints, resulting in physically suboptimal execution.

These two failure cases highlight the critical role of LLM reasoning capability in enabling successful flock formation. However, as shown in Fig. 10 and Fig. 11, strong reasoning alone is not sufficient—formation often fails without structured coordination. It is the combination of accurate plan generation and reliable motion execution, supported by our proposed influence-based consensus strategy, that leads to consistent and robust formation success.